

Geophysical Research Letters®



RESEARCH LETTER

10.1029/2024GL112439

Autotrophic Dissolved Organic Phosphorus Uptake Stimulates Nitrogen Fixation in Subtropical Gyres

Yuxin Shen¹ and Wei-Lei Wang¹ 

¹State Key Laboratory of Marine Environmental Science & College of Ocean and Earth Sciences, Xiamen University, Xiamen, China

Key Points:

- Autotrophic dissolved organic phosphorus (DOP) uptake supports 15% of marine net primary production (NPP), with nearly 60% from the subtropical gyres of the North Pacific and North Atlantic
- DOP utilization leads to a 9% increase in global N₂ fixation compared to the model without direct DOP utilization
- DOP utilization boosts the contribution of N₂ fixation to export production by 20%–40% in subtropical gyres

Supporting Information:

Supporting Information may be found in the online version of this article.

Correspondence to:

W.-L. Wang,
weilei.wang@xmu.edu.cn

Citation:

Shen, Y., & Wang, W.-L. (2025). Autotrophic dissolved organic phosphorus uptake stimulates nitrogen fixation in subtropical gyres. *Geophysical Research Letters*, 52, e2024GL112439. <https://doi.org/10.1029/2024GL112439>

Received 10 SEP 2024

Accepted 3 JAN 2025

Author Contributions:

Conceptualization: Wei-Lei Wang
Data curation: Yuxin Shen
Formal analysis: Yuxin Shen
Funding acquisition: Wei-Lei Wang
Investigation: Wei-Lei Wang
Methodology: Wei-Lei Wang
Resources: Wei-Lei Wang
Software: Yuxin Shen
Supervision: Wei-Lei Wang
Validation: Yuxin Shen, Wei-Lei Wang
Visualization: Yuxin Shen
Writing – original draft: Yuxin Shen, Wei-Lei Wang
Writing – review & editing: Wei-Lei Wang

© 2025. The Author(s).

This is an open access article under the terms of the [Creative Commons Attribution-NonCommercial-NoDerivs License](#), which permits use and distribution in any medium, provided the original work is properly cited, the use is non-commercial and no modifications or adaptations are made.

Abstract Dissolved organic phosphorus (DOP) has been identified as a key phosphorus source that supports primary production and microbial nitrogen (N₂) fixation. However, the specific contribution and spatial distribution of DOP utilization remain poorly understood due to limited in-situ measurements. In this study, we explored the role of DOP in supporting N₂ fixation using a modified inverse biogeochemical ocean model. Our findings reveal that DOP utilization primarily occurs in subtropical gyres, where it serves as a critical phosphorus source. Direct DOP assimilation reduces phosphorus limitation in nutrient-depleted gyres, thereby stimulating global N₂ fixation, the global distribution of which is re-estimated. The new estimate shows a significant increase in N₂ fixation rates in the North Atlantic compared to the previous estimate because DOP utilization reduces the severe phosphorus limitation in that region. Neglecting DOP utilization would result in an approximately 9% underestimation of the global N₂ fixation rate.

Plain Language Summary Dissolved organic phosphorus plays a crucial role in providing phosphorus, which is essential for primary production and microbial nitrogen (N₂) fixation. However, due to limited in-situ measurements, the extent and pattern of DOP use in the ocean are not well understood. In this study, we used a modified ocean model to investigate how DOP supports N₂ fixation. Our results show that DOP is mainly used in subtropical gyres, where it helps reduce phosphorus shortages, thereby boosting N₂ fixation globally. We found that N₂ fixation rates, especially in the North Atlantic, are much higher than previously thought due to the mitigating effect of DOP on phosphorus limitation. Ignoring the role of DOP would lead to an underestimation of global N₂ fixation by about 9%.

1. Introduction

Phosphorus (P) and nitrogen (N) are essential elements supporting primary production (Duhamel et al., 2021). However, in permanently stratified subtropical gyres, surface phosphate and nitrate concentrations are often lower than the theoretical uptake capacity of phytoplankton, thereby limiting the primary production (Wu et al., 2000; Yuan et al., 2023). Microbial dinitrogen (N₂) fixation, which draws atmospheric N₂ to produce bioavailable nitrogen, can fuel up to 50% of total productivity in certain regions (Louchard et al., 2021; Zehr & Capone, 2020). There are no external bioavailable sources like N₂ fixation in the marine phosphorus cycle. N₂ fixation is usually limited by the availability of phosphate and iron (Berman-Frank et al., 2001; Kustka et al., 2003; Wang et al., 2019; Wu et al., 2000). In regions such as the North Atlantic and the northern Indian Ocean, where high dust inputs reduce iron limitation, both field measurements and modeling studies reveal that N₂ fixation is primarily limited by phosphate availability (Sañudo-Wilhelmy et al., 2001; Wang et al., 2019). The lateral transport of DOP from productive poleward gyres and equatorial upwelling regions has been shown to supplement the phosphorus requirements of subtropical oceans, with the additional uptake of organic molecules liberating bioavailable P (Letscher et al., 2022). Laboratory experiments suggest that DOP utilization may be an external phosphorus source for N₂ fixation. The activity of Phosphodiesterase, an enzyme that helps hydrolyze P-ester, is positively correlated with the rates of N₂ fixation in the central North Pacific, which also implies that DOP may support N₂ fixation (Yamaguchi et al., 2019). Given that DOP concentrations often exceed those of dissolved inorganic phosphorus (DIP), DOP utilization could potentially alleviate phosphorus limitation for diazotrophs, thereby stimulating N₂ fixation, primary production, and export production. However, the specific contribution of DOP to N₂ fixation and its geographical distribution remain largely unknown.

The lack of quantification methods for DOP utilization efficiency limits our understanding of its contribution. Isotope incubation experiments, which measure only a specific type of DOP, cannot accurately reflect the overall

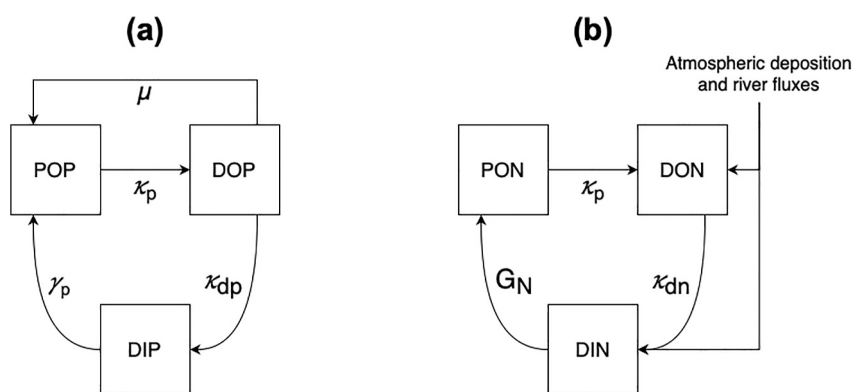


Figure 1. Schematic representation of (a) P-cycle and (b) N-cycle models. γ_p and μ are dissolved inorganic phosphorus and dissolved organic phosphorus (DOP) utilization rates that are defined in Section 2.1. κ_p is particulate organic phosphorus (POP) and particulate organic nitrogen dissolution rate constant and is prescribed to be $(1/30) \text{ d}^{-1}$. κ_{dp} and κ_{dn} are DOP and dissolved organic nitrogen remineralization rate constants, respectively. G_N is the dissolved inorganic nitrogen assimilation rate, which equals the product of the POP production rate ($\gamma_p[\text{DIP}] + \mu[\text{DOP}]$) and a spatial variable N:P ratio ($r_{\text{N:P}}$). Atmospheric deposition and river fluxes are prescribed in Section 2.2.

DOP assimilation rate (Karl, 2014). Alkaline phosphatase (AP), an enzyme that helps phytoplankton liberate bioavailable phosphorus from DOP molecules, serves as an indicator of DOP utilization. However, the presence of AP can only qualitatively suggest whether DOP is being utilized without quantifying the extent of DOP utilization. Moreover, AP can remain active for up to 2 weeks and, therefore, can be potentially transported away from the site of production (Cembella et al., 1984). This creates a spatiotemporal disconnect between in-situ AP activity and actual DOP utilization efficiency (Duhamel et al., 2021).

Due to the sparse global observations of DOP, extrapolating global distribution patterns is challenging. Biogeochemical models can estimate the contribution of DOP on a large scale by calculating elemental balances. Sensitivity tests using prognostic biogeochemical models have shown that global N_2 fixation increases by 26% in DOP utilization experiments compared to the control run (Letscher & Moore, 2015). However, uncertainties remain due to the dependence on prescribed model parameters. Inverse models, which deduce biogeochemical rates and fluxes constrained by observational data, offer a promising approach to reducing these uncertainties (DeVries, 2014; DeVries et al., 2012; Wang et al., 2023).

In this study, we use an inverse biogeochemically coupled N-P model, which is well-constrained by tens of thousands of hydrographic data points and effectively resolves the global nitrogen cycle (Wang et al., 2019). To investigate the impact of DOP uptake on N_2 fixation, a Monod equation is incorporated into the model to represent this mechanism as part of primary production. We present estimates on (a) the rate of DOP utilization in the global euphotic zone (EZ) and its contribution to NPP, (b) global patterns of N_2 fixation and the fraction supported by DOP utilization, and (c) the effect of DOP utilization and N_2 fixation on export production.

2. Methods

We modify the steady-state PN-cycling model from Wang et al., which has been used to diagnose spatial patterns of global N_2 fixation rates (Wang et al., 2019). In the revised phosphorus cycle (Figure 1), both inorganic and organic phosphorus are assimilated by phytoplankton to produce particulate organic phosphorus (POP). The net biological production of organic nitrogen is converted from phosphorus assimilation using a spatially variable N:P ratio as has been done before. After biological production, the labile part of the particles lyses and transforms to DOP.

2.1. Phosphorus Model

Three explicit tracers are considered in the phosphorus model: DIP, DOP, and POP. The governing equations for the phosphorus cycle are as follows:

$$\begin{aligned} \left[\frac{d}{dt} + \mathbf{T} \right] [\text{DIP}] &= -\gamma[\text{DIP}] + \kappa_{dp}[\text{DOP}] + \kappa_g([\text{DIP}] - \overline{[\text{DIP}]}_{\text{obs}}), \\ \left[\frac{d}{dt} + \mathbf{T} \right] [\text{DOP}] &= -\kappa_{dp}[\text{DOP}] + \kappa_p[\text{POP}] - \mu[\text{DOP}], \\ \left[\frac{d}{dt} + \mathbf{F} \right] [\text{POP}] &= \gamma[\text{DIP}] - \kappa_p[\text{POP}] + \mu[\text{DOP}], \end{aligned} \quad (1)$$

where \mathbf{T} is a transport matrix and is constrained using multiple tracers (DeVries & Holzer, 2019). $\mathbf{T}[\text{C}]$ represents advection (\vec{U}) and diffusion (\mathbf{K}) transport of dissolved tracer C ($\mathbf{T}[\text{C}] \equiv \nabla \cdot (\vec{U}[\text{C}] - \mathbf{K} \nabla [\text{C}])$). \mathbf{F} represents a sinking flux divergence operator. For example, $\mathbf{F}_{\text{POP}} \equiv \nabla \cdot (\vec{w}[\text{POP}])$, where \vec{w} is sinking speed and increases linearly with depth. The linearly increased sinking speed and a constant POP dissolution rate ($\kappa_p = 1/30 \text{ days}^{-1}$) produce a canonical power-law function:

$$F(z) = F(z_0) \left(\frac{z}{z_0} \right)^{-b}, \quad (2)$$

where $F(z)$ and $F(z_0)$ stand for fluxes at depth z and euphotic depth z_0 , respectively (Wang et al., 2019). κ_{dp} is DOP remineralization rate constant and is optimized in the inversion. κ_g is a geological restoring constant and is prescribed at $(1/10^6) \text{ yr}^{-1}$ to restore model mean concentration of DIP to observational mean value ($\overline{[\text{DIP}]}_{\text{obs}}$).

The biological production of organic phosphorus consists of two parts: DIP assimilation and autotrophic DOP uptake. Dissolved inorganic phosphorus assimilation rate is modeled using a spatially variable uptake rate coefficient ($\gamma(r)$, where r is a position coordinate), which is built using satellite-derived NPP (MODIS CbPM (Westberry et al., 2008)) and a gridded surface DIP observation ($[\text{DIP}]_{\text{obs}}$ from World Ocean Atlas 2018 (Garcia et al., 2019b)) as shown in Equation 3. We prescribe NPP_0 at $1 \text{ mmol C m}^{-2} \text{ s}^{-1}$ and $[\text{DIP}]_0$ at 1 mmol m^{-3} to remove the dimensions. α and β are scaling factors that are optimized in the inversion. $r_{\text{C:P}}$ is the C:P ratio according to Galbraith and Martiny (Galbraith & Martiny, 2015), and is used to convert NPP from C unit to P unit. Photosynthesis is limited to the EZ, the top two model layers ($z_0 = 73.4 \text{ m}$). The γ function is defined as follows:

$$\gamma(r) \equiv \begin{cases} \alpha \frac{\left[\frac{1}{r_{\text{C:P}}} \frac{\text{NPP}(r)}{\text{NPP}_0} \right]^\beta}{[\text{DIP}]_{\text{obs}}(r)}, & \text{if } z < z_0 \\ 0, & \text{otherwise} \end{cases}, \quad (3)$$

Dissolved organic phosphorus utilization is modeled according to Letscher et al. (2022), which is the reciprocal of the Monod equation with two adjustable parameters ν and k_m , the minimum uptake rate of DOP at elevated DIP concentration and half-saturation constant for maximal DOP uptake rate at low $[\text{DIP}]_{\text{obs}}$, respectively.

$$\mu = \nu \frac{(k_m + [\text{DIP}]_{\text{obs}})}{[\text{DIP}]_{\text{obs}}}. \quad (4)$$

2.2. Nitrogen Model

We simulate three nitrogen tracers, dissolved inorganic nitrogen (DIN), dissolved organic nitrogen (DON), and particulate organic nitrogen (PON) in the model. We use DIN to represent all bioavailable nitrogen (e.g., nitrate, nitrite, ammonia, urea). $r_{\text{N:P}}$ represents the non-Redfieldian N:P ratio, which is modeled using the following equation:

$$r_{\text{N:P}} = A + B\Theta([\text{DIP}]; [\text{DIP}]_c, \Omega), \quad (5)$$

where A and B are tunable parameters and are optimized in the inversion. Θ is a hyperbolic tangent function as defined by Equation 6. $[\text{DIP}]_c = 0 \text{ mmol m}^{-3}$ and $\Omega = 1 \text{ mmol m}^{-3}$ are prescribed because the model solution is not sensitive to them (Wang et al., 2019).

$$\Theta(x; x_c, \lambda) \equiv \frac{1}{2} \left[1 - \tanh\left(\frac{x - x_c}{\lambda}\right) \right], \quad (6)$$

The net biological production of organic phosphorus includes both inorganic (γ [DIP]) and organic phosphorus (μ [DOP]) utilization, which is then converted to organic nitrogen production by multiplying a ratio of nitrogen to phosphorus ($r_{\text{N:P}}$). The governing equations for the nitrogen cycle are as follows:

$$\begin{aligned} \left[\frac{d}{dt} + \mathbf{T} \right] [\text{DIN}] &= -r_{\text{N:P}}(\gamma[\text{DIP}] + \mu[\text{DOP}])\Lambda([\text{DIN}]) + \kappa_{dn}[\text{DON}] - (D_w + D_s) + (I_{riv} + I_{atm}), \\ \left[\frac{d}{dt} + \mathbf{T} \right] [\text{DON}] &= -\kappa_{dn}[\text{DON}] + \kappa_p[\text{PON}], \\ \left[\frac{d}{dt} + \mathbf{F} \right] [\text{PON}] &= r_{\text{N:P}}(\gamma[\text{DIP}] + \mu[\text{DOP}]) - \kappa_p[\text{PON}], \end{aligned} \quad (7)$$

where Λ is a hyperbolic tangent function defined according to Equation 6, which is used to gradually shut down DIN uptake when [DIN] is getting close to 0. The DIN threshold for initiating N_2 fixation is determined by optimal parameters constrained using field measurements of DIP, DIN, DOP, and DON. The optimal relationship between the N_2 -fixation-limiter ($1 - \Lambda(\text{DIN})$) and ambient DIN concentration is illustrated in Figure S1 in Supporting Information S1. N_2 fixation does not fully cease until ambient DIN reaches approximately $3.0 \mu\text{M}$. The actual nitrogen introduced through N_2 fixation is jointly determined by theoretical nitrogen uptake rate ($r_{\text{N:P}}(\gamma[\text{DIP}] + \mu[\text{DOP}])$) and the magnitude of the limiter (Equation 7), indicating that significant N_2 fixation can still occur in high-DIN waters if the nitrogen uptake rate is high, as is often the case in coastal regions (Selden et al., 2021; Tang, Wang, et al., 2019). Therefore, this modeling approach is effective for much of the open ocean and even some coastal oceans (Wang et al., 2019), but it may introduce bias in certain coastal regions, because previous studies have shown that N_2 fixation can occur even when ambient DIN concentrations are high ($>5.0 \mu\text{M}$) (Knapp, 2012; Mills et al., 2020). \mathbf{F} is the sinking flux divergence operator as mentioned in Section 2.1. D_w and D_s are water column denitrification and sedimentary denitrification, respectively, which are modeled as follows:

$$D_w = k_w \cdot \Theta([\text{O}_2]; [\text{O}_2]_c, \Delta) \cdot [\text{DOC}] \cdot [\text{DIN}], \quad (8)$$

$$D_s = \mathbf{B} \text{diag} \left(a_1 + a_2 \cdot \exp \left\{ c \left(\frac{[\text{O}_2] - [\text{DIN}]}{[\text{DIN}]_0} \right) \right\} \right) \mathbf{F}[\text{POC}], \quad (9)$$

where k_w and Δ are adjustable parameters and optimized in the inversion. The oxygen function limits denitrification to regions where oxygen levels are lower than the threshold value; DOC and POC are converted from DON and PON, respectively, using Redfield C:N ratio of 106:16; \mathbf{B} is a diagonal matrix symbolize the bottom of water columns where sediment denitrification occurs; $a_1 = 0.060$, $a_2 = 0.19$, $c = \log 0.99$, $[\text{DIN}]_0 = 1 \text{ mmol m}^{-3}$.

The atmospheric deposition (I_{atm}) and riverine inputs (I_{riv}) of nitrogen are prescribed for the current model exactly as in the previous model (see supplementary information of Wang et al., 2019). Since both models include these same external sources, they cancel out when we focus on comparing N_2 fixation driven by DOP utilization.

2.3. Observational Data

Observations of DIP, DOP, DIN, and DON are used to constrain model parameters. We download DIP and DIN data from the Global Ocean Data Analysis Project (GLODAPv2 (Olsen et al., 2016)), DOP from the DOPv2021 database (Liang et al., 2022), and DON from Letscher et al. (2015). Note that in this study only semi-labile DOP and DON whose lifetime spans from hours to months are considered. Refractory DON and DOP (rDON and rDOP, respectively) are adopted from Letscher and Moore (2015), who estimated the concentration of rDON and

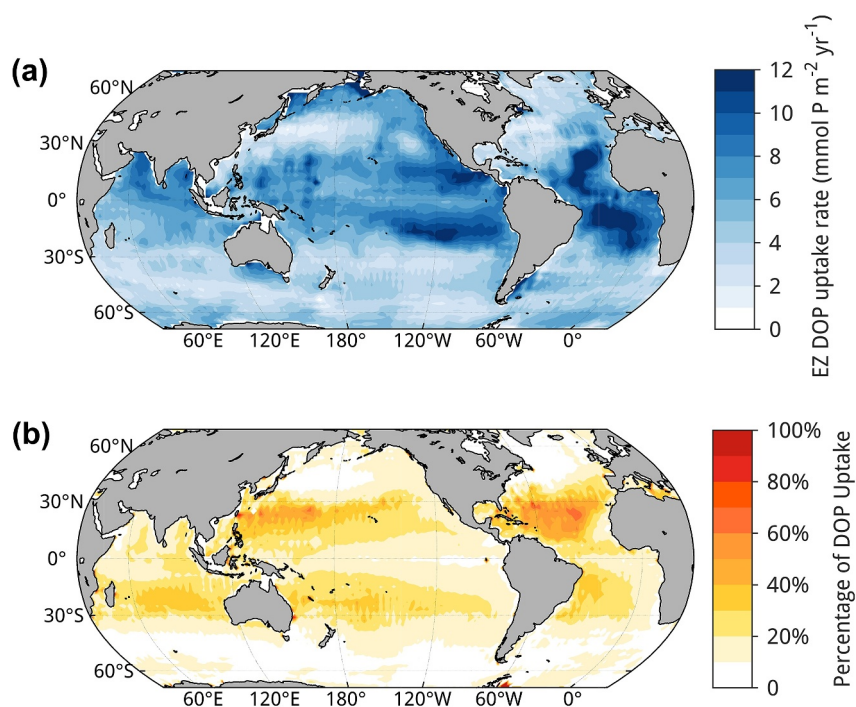


Figure 2. (a) Integrated euphotic zone dissolved organic phosphorus (DOP) uptake rate. (b) Contribution percentage of DOP uptake to net primary production, which is defined as dissolved inorganic phosphorus uptake plus autotrophic DOP uptake rate (see Section 2.1).

rDOP by identifying the asymptotic mean concentrations below 1,000 m from depth profiles of DON and DOP measurements. No spatial variations of refractory DON ($1.8 \pm 0.4 \mu\text{M}$) and DOP ($0.03 \pm 0.02 \mu\text{M}$) were found possibly owing to large analytical error of deep ocean DON and DOP measurements (Letscher & Moore, 2015). We update rDOP concentration to $0.05 \mu\text{M}$ according to Liang et al. (2022) with an updated DOP data ($\sim 3,800$ observations). Therefore, we subtract the refractory DOP of $0.05 \mu\text{M}$ and refractory DON of $1.8 \mu\text{M}$ from observations to obtain ‘semi-labile’ DOP and DON. Furthermore, oxygen data from World Ocean Atlas (Garcia et al., 2019a) are used to build the denitrification function as described in Section 2.2. The optimization routine used in this study follows the approach outlined by Wang et al. (2019), which reproduces the observational data well (Figure S2 in Supporting Information S1).

3. Results and Discussion

3.1. Global Distribution of Dissolved Organic Phosphorus Uptake

The vertically integrated autotrophic DOP uptake rate in the EZ increases from nutrient-rich subpolar regions to nutrient-poor subtropical gyres (Figure 2a). High DOP utilization rates are observed in the central North and South Atlantic Oceans, as well as in the tropical northeastern and southeastern Pacific oceans. However, the reasons leading to high rates of DOP uptake may differ. The high rates in the North Atlantic Oceans are attributed to the consistently low DIP concentrations (Dai et al., 2023), whereas the elevated levels in the South Atlantic Ocean, the eastern tropical North and South Pacific Oceans are likely due to the high phosphorus demand driven by the intense primary production.

High rates of DOP uptakes are also found in coastal systems, likely influenced by species-level resource partitioning (Alexander et al., 2016; Schoffelen et al., 2018), that is, species capable of hydrolyzing DOP exhibit a competitive advantage over those lacking this ability. For example, there are hot spots in nearshore areas such as southern Australia and the Bering Strait. However, these findings should be interpreted with caution due to the coarse resolution of the model. Elevated utilization rates are particularly prominent along the flanks of the eastern upwelling systems in the Atlantic and Pacific Oceans. The North Atlantic Subtropical Gyre (NASG), where depleted DIP severely limits phytoplankton growth, particularly diazotrophs (Moore et al., 2013), exhibits the

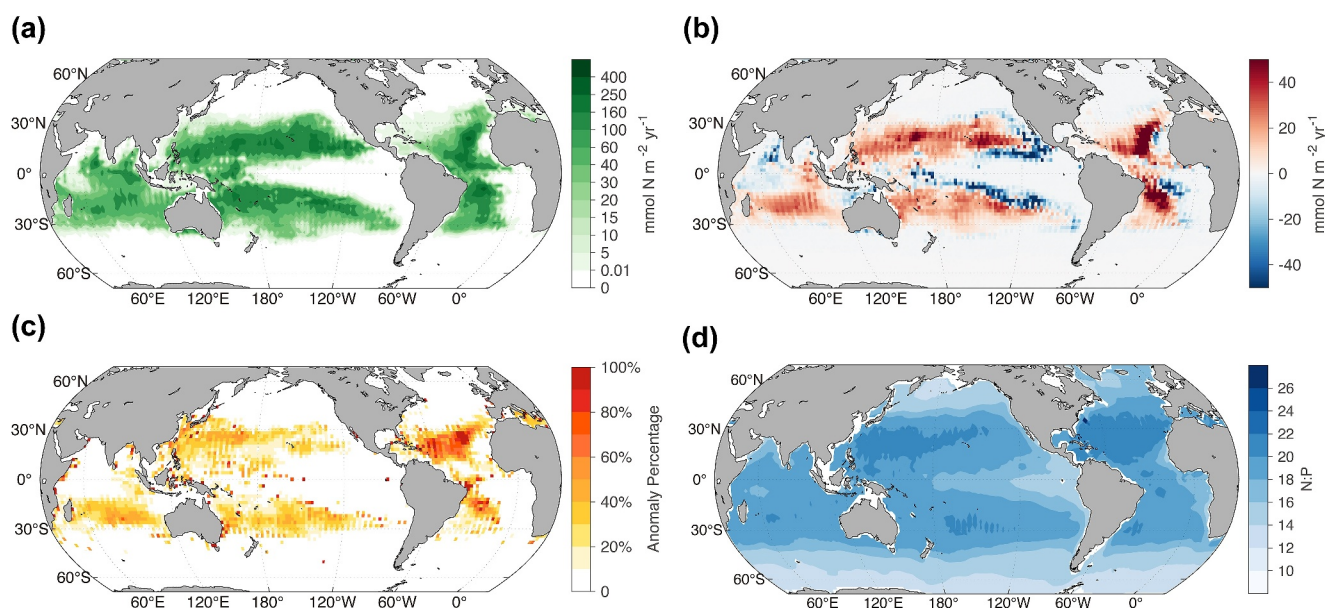


Figure 3. (a) Global distribution of microbial N₂ fixation rate. (b) N₂ fixation anomaly. Anomaly is the difference between the dissolved organic phosphorus (DOP) absorption model (this research) and the model without it (Wang et al., 2019). (c) N₂ fixation anomaly in percentage, which is the ratio between the absolute anomaly (b) and N₂ fixation rate (a). To emphasize the relative contributions of DOP utilization to N₂ fixation, only positive anomalies are considered, while negative ones are disregarded. (d) N:P ratio of exported particles from the euphotic zone (EZ). Here we calculated particulate organic material exported from the EZ (73.4 m, the first two model layers) to deeper layers.

highest DOP uptake rate (~ 12 mmol P m⁻² yr⁻¹). This notable assimilation differs from previous research (Letscher et al., 2022), but we consider it reliable given the strong phosphorus limitation in this region, which suggests the presence of compensatory mechanisms among phytoplankton.

Autotrophic DOP uptake supports 15% of global NPP. Surprisingly, the highest contribution percentages ($\sim 60\%$ – 70%) were found in the western subtropical gyres of both the Pacific and Atlantic Oceans (Figure 2b), despite lower DOP assimilation rates in these regions compared to the eastern basins (Figure 2a). The discrepancy can be explained by different nutrient supply mechanisms: upwelling systems along the eastern boundaries bring abundant nutrients (e.g., DIP) from the subsurface to the surface, thereby supporting higher primary production in these eastern basins. Phytoplankton community in downstream areas that lacks supply from the subsurface uses DOP as a compensatory. In the Indian Ocean, the highest DOP assimilation rates are observed in the northern basins, such as the Bay of Bengal and the Arabian Sea. At the same time, DOP supports a higher fraction of NPP in the southern subtropical Indian Ocean for reasons like those in the Pacific and Atlantic oceans. In summary, DOP uptake is a vital phosphorus source in subtropical gyres, with the highest assimilation rates in the eastern gyres but supporting a greater fraction of NPP in the western and central gyres.

3.2. Dissolved Organic Phosphorus Uptake Stimulates N₂ Fixation

We update the estimate on the global microbial N₂ fixation rate with DOP as an additional phosphorus source. The new global estimate is 176 Tg N yr⁻¹ which is on average $\sim 9\%$ higher compared to the previous model results (Wang et al., 2019). Our globally integrated estimate of N₂ fixation (176 Tg N yr⁻¹) falls into the range estimated by previous models (133 ± 72 Tg N yr⁻¹) (Tang, Li, et al., 2019) and is closer to the arithmetic mean (223 ± 30 Tg N yr⁻¹) derived from extrapolation of in-situ observations (Shao et al., 2023) compared to our previous estimate (163 Tg N yr⁻¹) (Wang et al., 2019). Spatially, the general pattern of N₂ fixation rate is similar to that from the previous results (Wang et al., 2019). High rates of N₂ fixation mainly occur in the subtropical gyres downstream of eastern boundary upwelling systems (Figure 3a), low rates are found in the high-latitude oceans and eastern equatorial upwelling systems. The spatial pattern aligns with field measurements (Bonnet et al., 2017). The combined N₂ fixation and external inputs (atmospheric and riverine inputs) deliver 212 Tg N yr⁻¹ to the ocean, which are balanced by nitrogen losses via denitrification and anaerobic ammonium oxidation (anammox) in the water column (63 Tg N yr⁻¹) and sediment (150 Tg N yr⁻¹). The water column

nitrogen loss rate aligns well with the previous report (DeVries et al., 2013), while benthic nitrogen loss is higher than the former estimation ($131.5 \text{ Tg N yr}^{-1}$) to compensate for higher N input (Wang et al., 2019).

We quantified the contribution of DOP to N_2 fixation by calculating the difference between the outputs of our modified model and previous results that did not include direct DOP utilization, which is identified as the 'anomaly' in Figure 3b. The positive anomaly (Figure 3b) occurs in central gyres, where direct DOP utilization provides an additional phosphorus source beyond DIP (Figure 2b). The percentage of positive anomalies reveals the relative contribution of DOP utilization to N_2 fixation across different basins (Figure 3c). In the western gyres, although the absolute rates of DOP utilization are low, its contribution to NPP and N_2 fixation is relatively high compared to the eastern basins. In the NASG, N_2 fixation rates nearly double, indicating that the direct utilization of DOP alleviates the severe phosphorus limitation.

Consistent with earlier model outputs, negative anomalies in N_2 fixation (Figure 3b) are found along the edges of equatorial upwelling systems in both the Pacific and Atlantic oceans (Letscher & Moore, 2015). These upwelling systems are crucial in supplying nutrients to subtropical gyres through large-scale cyclonic circulations. In the previous model, N_2 fixation in the central gyres was limited by low phosphate concentrations, necessitating the import of nitrate from the edges of the gyres to sustain primary production, thereby promoting higher N_2 fixation rates at the edges. However, with the direct utilization of DOP in the gyres, the dependence on nitrate from the edges is reduced, leading to lower N_2 fixation rates as inferred from the model. A similar pattern is observed in the Indian Ocean: the equatorial and southern regions, where DOP utilization dominates (>50% of NPP, Figure 2b), exhibit a positive anomaly, while the northern Indian Ocean shows a slight negative anomaly.

High N_2 fixation rates in the subtropical gyres lead to a higher N:P ratio than the Redfield value in exported organic matter (Figure 3d). The N:P ratios in exported organic particles can be up to approximately 20:1 in subtropical gyres. In contrast, denitrification in the Oxygen Minimum Zones (OMZs) of the eastern Pacific and eastern Atlantic reduces the ratio to around 14:1. The incorporation of DOP utilization results in a higher N:P ratio in exported material compared to the previous model that does not account for DOP utilization. The positive anomaly increases from 0.1 at the edge of the gyre to 0.5 in the center. Conversely, intensified denitrification lowers the N:P ratio in the OMZs, while enhanced N_2 fixation in the subtropical gyres raises the N:P ratio. Together, these processes help maintain a relatively constant global mean N:P ratio. The N:P ratio in exported organic particles aligns well with field observations (Martiny et al., 2014) (Figure S3 in Supporting Information S1). However, please note that this is not a direct comparison, as the modeled N:P ratio represents sinking PON/POP at the base of the model EZ (73 m), while the measured PON/POP ratios are for suspended particles within the EZ (0–100 m). Due to the limited availability of field measurements on export PON/POP ratios, this comparison is the best approximation available.

3.3. Contribution of Dissolved Organic Phosphorus Uptake and N_2 Fixation to Export Production

Globally integrated Annual Net Community Production (ANCP) is $10.5 \text{ Pg C yr}^{-1}$ in our estimation assuming a constant C/N ratio (106:16), which is calculated by subtracting the EZ's organic nitrogen remineralization from primary production. Our result is close to the non-advective-diffusive POC vertical flux estimation, which is $10.63 \text{ Pg C yr}^{-1}$ (Wang et al., 2023). In the subtropical ocean, our estimated ANCP rate (Figure 4a and Figure S4 in Supporting Information S1) is higher in both flanks of eastern upwelling systems in the Pacific and the Atlantic, where an elevated DOP utilization rate is shown (Figure 2a). For comparison, export flux concentrated in coastal regions in the previous research. The difference underlies the intensifying contribution of DOP utilization on export production. Our ANCP estimate for the eastern equatorial Pacific ($3.5\text{--}4 \text{ mol C m}^{-2} \text{ yr}^{-1}$) (Figure S4 in Supporting Information S1) aligns well with the satellite-based ANCP ($3\text{--}4 \text{ mol C m}^{-2} \text{ yr}^{-1}$) (Yang et al., 2019). In the southern flanks of the eastern upwelling system ($\sim 15^\circ\text{S}$), our estimation is slightly higher ($4\text{--}4.5 \text{ mol C m}^{-2} \text{ yr}^{-1}$ compared to $2.5\text{--}3.5 \text{ mol C m}^{-2} \text{ yr}^{-1}$), presumably due to the utilization of DOP. High export flux is observed in the subpolar Southern Ocean, North Pacific, and North Atlantic, consistent with the previous study (Wang et al., 2023).

In N-depleted subtropical gyres, newly fixed nitrogen is a crucial nitrogen source for export production. The percentage of new nitrogen contributing to export production increases from $\sim 30\%$ at the edges to $\sim 100\%$ in the central gyres (Figure 4b). The general pattern of an increasing contribution of N_2 fixation to export/new production from the edges to the center of gyres aligns with field measurements using isotope tracers by

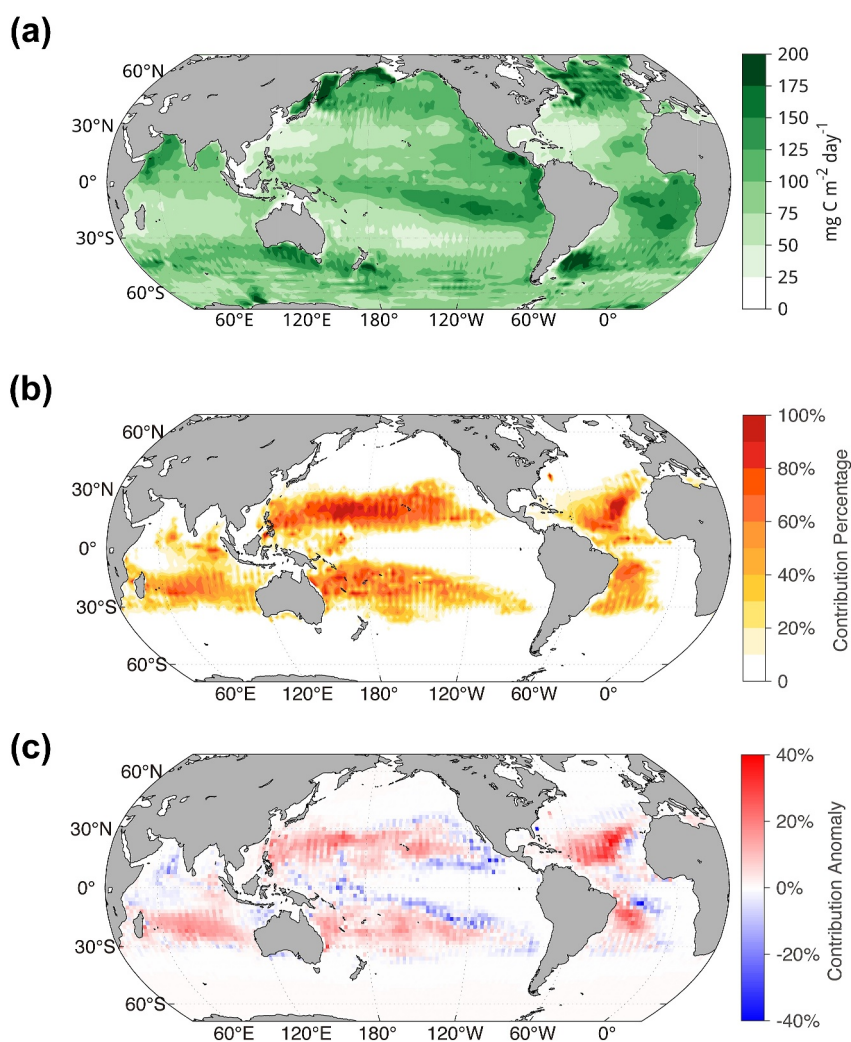


Figure 4. (a) Annual Net Community Production (ANCP). ANCP is calculated by gross biological production (N assimilation) minus respiration in the euphotic zone and multiplied by the constant C:N ratio. (b) Contribution of newly fixed N to export production. (c) Anomaly of contributions of newly fixed N to export production. Anomaly is the difference between the dissolved organic phosphorus absorption model (this research) and the model neglecting it (Wang et al., 2019).

Shiozaki et al. (2009). However, the specific percentage contributions differ, likely due to variations in export depth selection (e.g., uniformly 73 m in our model vs. measurement depth defined by 1% photosynthetically active radiation). The relative contribution of new nitrogen to export production in our estimates (72%) is close to the measurements at Station ALOHA, where newly fixed nitrogen accounts for 36%–69% of export/new production (Dore et al., 2002). The consistent distribution of new nitrogen contribution (Figure 4b) and N_2 fixation rate (Figure 3a) underscores the importance of N_2 fixation for new production.

To quantify the effect of DOP utilization on export production, we compare the contribution percentages between models with and without DOP assimilation. The difference shown in Figure 4c, highlights the contribution of DOP utilization to ANCP. Dissolved organic phosphorus utilization leads to a $\sim 20\%$ increase in the Pacific and southern Indian Oceans and a $\sim 40\%$ increase in the Atlantic. In conclusion, DOP utilization is vital for N_2 fixation and primary production in subtropical gyres (Figure 2b). By alleviating phosphorus limitation, microbial N_2 fixation is enhanced (Figure 3b), which in turn boosts export production (Figure 4c).

4. Conclusions

We have quantified the contribution of DOP utilization to microbial N_2 fixation by modifying the inverse biogeochemical N-P model to include a DOP utilization function. Our results reveal that DOP assimilation enhances microbial N_2 fixation, and that a large fraction of the NPP in subtropical gyres is supported by DOP utilization with contributions ranging from $\sim 40\%$ at the edges to $\sim 100\%$ in the center (Figure 2b). This indicates that DOP utilization is a crucial mechanism for obtaining additional phosphorus in P-depleted gyres. As phosphorus limitation is alleviated, microbial N_2 fixation is enhanced, with the global integrated rate increasing by $\sim 9\%$ compared to previous model that did not account for DOP utilization. Regionally, in the NASG, which experiences severe phosphorus limitation, microbial N_2 fixation rates show a $\sim 100\%$ increase. Both DOP utilization and microbial N_2 fixation are critical for new production, with DOP utilization contributing to a $\sim 20\%$ – 40% increase in the contribution of newly fixed nitrogen to export production in subtropical gyres. However, our model does have some limitations. For instance, we simplify the diverse DOP compounds into a single group and optimize a global mean e-folding remineralization rate constant for DOP. Additionally, we have not accounted for aerosol-derived DOP, which may moderately underestimate DOP utilization in the NASG (Jin et al., 2024). Finally, the model resolution is relatively low and lacks seasonal variability.

In the future, development of high-resolution inverse models will allow us to better capture the complexities of nitrogen and phosphorus cycling in coastal regions, particularly to represent the high N_2 fixation rates observed in field studies (Tang, Wang, et al., 2019). Additionally, incorporation of seasonal resolution in these models will help capture the seasonal fluctuations in DOP concentrations observed at stations such as ALOHA and BATS (Church et al., 2002; Lomas et al., 2010), providing a more comprehensive understanding of DOP dynamics.

Data Availability Statement

The new estimate on global scale oceanic N_2 fixation and associated data to generate the figures in this study are available at Zenodo (Wang & Shen, 2024). The code for the modified oceanic N-P model is available at Zenodo (Shen & Wang, 2024).

References

- Alexander, H., Jenkins, B. D., Rynearson, T. A., & Dyhrman, S. T. (2016). Metatranscriptome analyses indicate resource partitioning between diatoms in the field (vol 112, pg E2182, 2015). *Proceedings of the National Academy of Sciences of the United States of America*, 113(25), E3589. <https://doi.org/10.1073/pnas.1608043113>
- Berman-Frank, I., Cullen, J. T., Shaked, Y., Sherrell, R. M., & Falkowski, P. G. (2001). Iron availability, cellular iron quotas, and nitrogen fixation in *Trichodesmium*. *Limnology & Oceanography*, 46(6), 1249–1260. <https://doi.org/10.4319/lo.2001.46.6.1249>
- Bonnet, S., Caffin, M., Berthelot, H., & Moutin, T. (2017). Hot spot of N_2 fixation in the western tropical South Pacific pleads for a spatial decoupling between N_2 fixation and denitrification. *Proceedings of the National Academy of Sciences of the United States of America*, 114(14), E2800–E2801. <https://doi.org/10.1073/pnas.1619514114>
- Cembella, A. D., Antia, N. J., & Harrison, P. J. (1984). The utilization of inorganic and organic phosphorous compounds as nutrients by eukaryotic microalgae: A multidisciplinary perspective: Part 1. *Critical Reviews in Microbiology*, 10(4), 317–391. <https://doi.org/10.3109/10408418209113567>
- Church, M. J., Ducklow, H. W., & Karl, D. M. (2002). Multiyear increases in dissolved organic matter inventories at station ALOHA in the North Pacific Subtropical Gyre. *Limnology & Oceanography*, 47(1), 1–10. <https://doi.org/10.4319/lo.2002.47.1.0001>
- Dai, M. H., Luo, Y. W., Achterberg, E. P., Browning, T. J., Cai, Y. H., Cao, Z. M., et al. (2023). Upper Ocean biogeochemistry of the oligotrophic North Pacific subtropical gyre: From nutrient sources to carbon export. *Reviews of Geophysics*, 61(3). <https://doi.org/10.1029/2022RG000800>
- DeVries, T. (2014). The oceanic anthropogenic CO₂ sink: Storage, air-sea fluxes, and transports over the industrial era [Article]. *Global Biogeochemical Cycles*, 28(7), 631–647. <https://doi.org/10.1002/2013gb004739>
- DeVries, T., Deutsch, C., Raftar, P. A., & Primeau, F. (2013). Marine denitrification rates determined from a global 3-D inverse model. *Biogeochemistry*, 10(4), 2481–2496. <https://doi.org/10.5194/bg-10-2481-2013>
- DeVries, T., & Holzer, M. (2019). Radiocarbon and helium isotope constraints on deep ocean ventilation and mantle-He sources. *Journal of Geophysical Research-Oceans*, 124(5), 3036–3057. <https://doi.org/10.1029/2018jc014716>
- DeVries, T., Primeau, F., & Deutsch, C. (2012). The sequestration efficiency of the biological pump. *Geophysical Research Letters*, 39(13). <https://doi.org/10.1029/2012gl051963>
- Dore, J. E., Brum, J. R., Tupas, L. M., & Karl, D. M. (2002). Seasonal and interannual variability in sources of nitrogen supporting export in the oligotrophic subtropical North Pacific Ocean. *Limnology and Oceanography*, 47(6), 1595–1607.
- Duhamel, S., Diaz, J. M., Adams, J. C., Djaoudi, K., Steck, V., & Waggoner, E. M. (2021). Phosphorus as an integral component of global marine biogeochemistry. *Nature Geoscience*, 14(6), 359–368. <https://doi.org/10.1038/s41561-021-00755-8>
- Galbraith, E. D., & Martiny, A. C. (2015). A simple nutrient-dependence mechanism for predicting the stoichiometry of marine ecosystems. *Proceedings of the National Academy of Sciences of the U S A*, 112(27), 8199–8204. <https://doi.org/10.1073/pnas.1423917112>
- Garcia, H., Weathers, K., Paver, C., Smolyar, I., Boyer, T., Locarnini, R., et al. (2019a). NOAA Atlas NESDIS 83 WORLD OCEAN ATLAS 2018 volume 3: Dissolved oxygen, apparent oxygen utilization, and dissolved oxygen saturation NOAA national centers for environmental information NOAA Atlas NESDIS 83.

Acknowledgments

We thank the thousands of scientists and researchers who made nutrient measurements. We also thank the people and institutes who maintain the public data repositories (GLODAP and WOA) and the Ocean Productivity website maintained by Oregon State University. W.-L.W and Y.S. were supported by the National Key Research and Development Program of China (2023YFF0805004), the National Natural Science Foundation of China (42476031), and the Natural Science Foundation of Fujian Province of China (2023J02001).

- Garcia, H., Weathers, K., Paver, C., Smolyar, I., Boyer, T., Locarnini, R., et al. (2019b). NOAA Atlas NESDIS 84 WORLD OCEAN ATLAS 2018 volume 4: Dissolved inorganic nutrients (phosphate, nitrate and nitrate+nitrite, silicate) NOAA national centers for environmental information WORLD OCEAN ATLAS 2018 volume 4: Dissolved inorganic nutrients (phosphate, nitrate and nitrate+nitrite, silicate).
- Jin, H. Y., Zhang, C., Meng, S. Y., Wang, Q., Ding, X. K., Meng, L., et al. (2024). Atmospheric deposition and river runoff stimulate the utilization of dissolved organic phosphorus in coastal seas. *Nature Communications*, *15*(1), 658. <https://doi.org/10.1038/s41467-024-44838-7>
- Karl, D. M. (2014). Microbially mediated transformations of phosphorus in the sea: New views of an old cycle. *Annual Review of Marine Science*, *6*(6), 279–337. <https://doi.org/10.1146/annurev-marine-010213-135046>
- Knapp, A. N. (2012). The sensitivity of marine N₂ fixation to dissolved inorganic nitrogen. *Frontiers in Microbiology*, *3*. <https://doi.org/10.3389/fmicb.2012.00374>
- Kustka, A. B., Sañudo-Wilhelmy, S. A., Carpenter, E. J., Capone, D., Burns, J., & Sunda, W. G. (2003). Iron requirements for dinitrogen- and ammonium-supported growth in cultures of (IMS 101): Comparison with nitrogen fixation rates and iron: Carbon ratios of field populations. *Limnology & Oceanography*, *48*(5), 1869–1884. <https://doi.org/10.4319/lo.2003.48.5.1869>
- Letscher, R. T., & Moore, J. K. (2015). Preferential remineralization of dissolved organic phosphorus and non-Redfield DOM dynamics in the global ocean: Impacts on marine productivity, nitrogen fixation, and carbon export. *Global Biogeochemical Cycles*, *29*(3), 325–340. <https://doi.org/10.1002/2014gb004904>
- Letscher, R. T., Moore, J. K., Teng, Y. C., & Primeau, F. (2015). Variable C: N: P stoichiometry of dissolved organic matter cycling in the community earth system model. *Biogeosciences*, *12*(1), 209–221. <https://doi.org/10.5194/bg-12-209-2015>
- Letscher, R. T., Wang, W. L., Liang, Z., & Knapp, A. N. (2022). Regionally variable contribution of dissolved organic phosphorus to marine annual net community production. *Global Biogeochemical Cycles*, *36*(12). <https://doi.org/10.1029/2022GB007354>
- Liang, Z., McCabe, K., Fawcett, S., Forrer, H., Hashihama, F., Jeandel, C., et al. (2022). A global ocean dissolved organic phosphorus concentration database (DOPv2021). *Scientific Data*, *9*(1), 772. <https://doi.org/10.1038/s41597-022-01873-7>
- Lomas, M. W., Burke, A. L., Lomas, D. A., Bell, D. W., Shen, C., Dyrhman, S. T., & Ammerman, J. W. (2010). Sargasso Sea phosphorus biogeochemistry: An important role for dissolved organic phosphorus (DOP). *Biogeosciences*, *7*(2), 695–710. <https://doi.org/10.5194/bg-7-695-2010>
- Louchard, D., Gruber, N., & Münnich, M. (2021). The impact of the amazon on the biological pump and the air-sea CO₂ balance of the western tropical atlantic. *Global Biogeochemical Cycles*, *35*(6). <https://doi.org/10.1029/2020GB006818>
- Martiny, A. C., Vrugt, J. A., & Lomas, M. W. (2014). Concentrations and ratios of particulate organic carbon, nitrogen, and phosphorus in the global ocean. *Scientific Data*, *1*, 140048. <https://doi.org/10.1038/sdata.2014.48>
- Mills, M. M., Turk-Kubo, K. A., van Dijken, G. L., Henke, B. A., Harding, K., Wilson, S. T., et al. (2020). Unusual marine cyanobacteria/haptophyte symbiosis relies on N₂ fixation even in N-rich environments. *ISME Journal*, *14*(10), 2395–2406. <https://doi.org/10.1038/s41396-020-0691-6>
- Moore, C. M., Mills, M. M., Arrigo, K. R., Berman-Frank, I., Bopp, L., Boyd, P. W., et al. (2013). Processes and patterns of oceanic nutrient limitation. *Nature Geoscience*, *6*(9), 701–710. <https://doi.org/10.1038/Ngeo1765>
- Olsen, A., Key, R. M., van Heuven, S., Lauvset, S. K., Velo, A., Lin, X., et al. (2016). The Global Ocean Data analysis Project version 2 (GLODAPv2) – An internally consistent data product for the World Ocean. *Earth System Science Data*, *8*(2), 297–323. <https://doi.org/10.5194/essd-8-297-2016>
- Sañudo-Wilhelmy, S. A., Kustka, A. B., Gobler, C. J., Hutchins, D. A., Yang, M., Lwiza, K., et al. (2001). Phosphorus limitation of nitrogen fixation by *Trichodesmium* in the central Atlantic Ocean. *Nature*, *411*(6833), 66–69. <https://doi.org/10.1038/35075041>
- Schoffelen, N. J., Mohr, W., Ferdelman, T. G., Littmann, S., Duerschlag, J., Zubkov, M. V., et al. (2018). Single-cell imaging of phosphorus uptake shows that key harmful algae rely on different phosphorus sources for growth. *Scientific Reports*, *8*(1), 17182. <https://doi.org/10.1038/s41598-018-35310-w>
- Selden, C. R., Chappell, P. D., Clayton, S., Macías-Tapia, A., Bernhardt, P. W., & Mulholland, M. R. (2021). A coastal N₂ fixation hotspot at the Cape Hatteras front: Elucidating spatial heterogeneity in diazotroph activity via supervised machine learning. *Limnology & Oceanography*, *66*(5), 1832–1849. <https://doi.org/10.1002/lno.11727>
- Shao, Z., Xu, Y., Wang, H., Luo, W., Wang, L., Huang, Y., et al. (2023). Global oceanic diazotroph database version 2 and elevated estimate of global oceanic N₂ fixation. *Earth System Science Data*, *15*, 3673–3709.
- Shen, Y. X., & Wang, W. L. (2024). Matlab code for “autotrophic dissolved organic phosphorus uptake Stimulates nitrogen fixation in subtropical gyres” by shen, yuxin and Wang, wei-lei. *Zenodo*. [Software]. <https://doi.org/10.5281/zenodo.14122542>
- Shiozaki, T., Furuya, K., Kodama, T., & Takeda, S. (2009). Contribution of N₂ fixation to new production in the western North Pacific Ocean along 155°E. *Marine Ecology Progress Series*, *377*, 19–32. <https://doi.org/10.3354/meps07837>
- Tang, W. Y., Li, Z. C., & Cassar, N. (2019a). Machine learning estimates of global marine nitrogen fixation. *Journal of Geophysical Research-Biogeosciences*, *124*(3), 717–730. <https://doi.org/10.1029/2018jg004828>
- Tang, W. Y., Wang, S., Fonseca-Batista, D., Dehairs, F., Gifford, S., Gonzalez, A. G., et al. (2019b). Revisiting the distribution of oceanic N₂ fixation and estimating diazotrophic contribution to marine production. *Nature Communications*, *10*(1), 831. <https://doi.org/10.1038/s41467-019-08640-0>
- Wang, W. L., Fu, W., Le Moigne, F. A. C., Letscher, R. T., Liu, Y., Tang, J. M., & Primeau, F. W. (2023). Biological carbon pump estimate based on multidecadal hydrographic data. *Nature*, *624*(7992), 579–585. <https://doi.org/10.1038/s41586-023-06772-4>
- Wang, W. L., Moore, J. K., Martiny, A. C., & Primeau, F. W. (2019). Convergent estimates of marine nitrogen fixation. *Nature*, *566*(7743), 205–211. <https://doi.org/10.1038/s41586-019-0911-2>
- Wang, W. L., & Shen, Y. X. (2024). Data used to generate figures in 'autotrophic dissolved organic phosphorus uptake Stimulates nitrogen fixation in subtropical gyres'. *Zenodo*. [Dataset]. <https://doi.org/10.5281/zenodo.13743686>
- Westberry, T., Behrenfeld, M. J., Siegel, D. A., & Boss, E. (2008). Carbon-based primary productivity modeling with vertically resolved photoacclimation. *Global Biogeochemical Cycles*, *22*(2). <https://doi.org/10.1029/2007gb003078>
- Wu, J. F., Sunda, W., Boyle, E. A., & Karl, D. M. (2000). Phosphate depletion in the western North Atlantic ocean. *Science*, *289*(5480), 759–762. <https://doi.org/10.1126/science.289.5480.759>
- Yamaguchi, T., Sato, M., Hashihama, F., Ehama, M., Shiozaki, T., Takahashi, K., & Furuya, K. (2019). Basin-scale variations in labile dissolved phosphoric monoesters and diesters in the central North Pacific ocean. *Journal of Geophysical Research-Oceans*, *124*(5), 3058–3072. <https://doi.org/10.1029/2018jc014763>
- Yang, B., Emerson, S. R., & Quay, P. D. (2019). The subtropical ocean's biological carbon pump determined from O₂ and DIC/DI¹³C tracers. *Geophysical Research Letters*, *46*(10), 5361–5368. [Article]. <https://doi.org/10.1029/2018gl01239>

- Yuan, Z. W., Browning, T. J., Zhang, R. F., Wang, C. W., Du, C. J., Wang, Y. M., et al. (2023). Potential drivers and consequences of regional phosphate depletion in the western subtropical North Pacific. *Limnology and Oceanography Letters*, 8(3), 509–518. <https://doi.org/10.1002/lol2.10314>
- Zehr, J. P., & Capone, D. G. (2020). Changing perspectives in marine nitrogen fixation. *Science*, 368(6492), 729. <https://doi.org/10.1126/science.aay9514>